RSC Advances




ROYAL SOCIETY OF CHEMISTRY

www.rsc.org/advances

Graphical Abstract

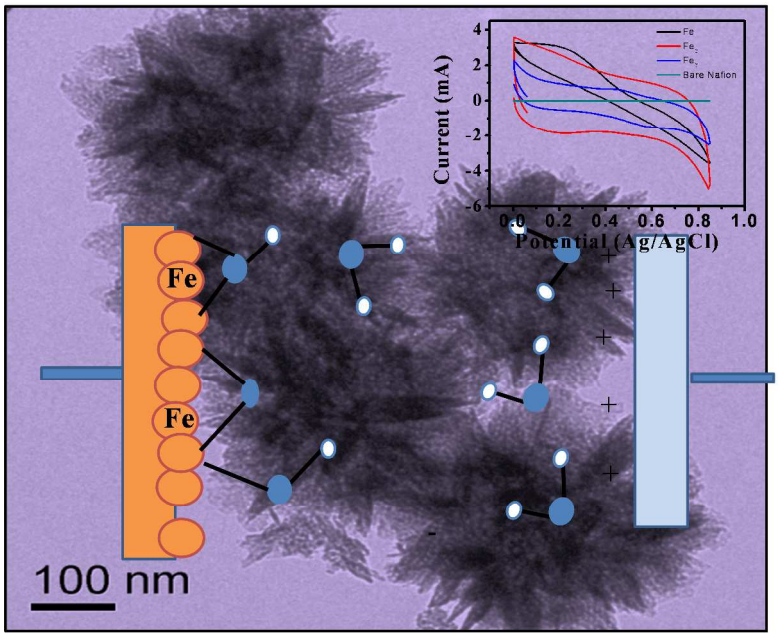

RSC Advance

RSCPublishing

ARTICLE

# In-situ synthesis of flowery shape α-FeOOH/$Fe_2O_3$ nano particles and their phase dependant supercapacitive behaviour

Cite this: DOI: 10.1039/x0xx00000x

Received 00th Feb 2014,
Accepted 00th Feb 2014

DOI: 10.1039/x0xx00000x

www.rsc.org/

Rasmita Barik[a], Bikash Kumar Jena[a], Ajit Dash[a], Mamata Mohapatra[a]*

Insitu one step facile synthetic strategies for flowery shape iron oxides nanoparticles were developed. Here in, we report simplified controlled synthesis of 2Line ferrihydrite- goethite core shell particles for the 1st time in semi aqueous-organic medium. The present route offered phase selectivity by controlling only the ratio of aqueous to organic phase. As synthesised nanoparticles have high surface area of 110$m^2$/g and 185$m^2$/g for 2line ferrihydrite and core shell goethite respectively. Further flowery shape hematite nano particles were obtained by annealing core shell iron oxides at 400°C. Phase purities were confirmed by XRD (X-Ray diffraction study), IR (infrared spectroscopy), and XPS (X-Ray photo electron spectroscopy) analysis. Formation of core shell nano structure for the iron oxide was confirmed by Mössbauer and SAED(selected area electron diffraction)studies. All the synthesized iron oxide materials were used to study their supercapacitor application by cyclic voltammetry (CV), electrochemical impedance spectroscopy (EIS), and chrono-potentiometry charge–discharge measurements. Specific capacitances for core shell α-FeOOH and α-$Fe_2O_3$ were found to be 160F/g and 200F/g respectively. These values were much higher as compared to the previous reported values for pure phases of iron oxides. The chrono-potentiometric charge–discharge study for all the three samples reveals their self-discharging capacity. Moreover, these iron oxide composite electrodes had also exhibited excellent cycling performance with >99% capacitance retention over 500 cycles. The electrochemical performance in two electrode system had also included. Furthermore, the electrochemical impedance spectroscopy (EIS) demonstrates the electrochemical resistance of α-$Fe_2O_3$ was slightly reduced with number of cycle, indicating easier access for intercalation/deintercalation of charges in the flowery structured materials. Thus the present material can be used as electrochemical supercapacitor for futuristic high-performance energy storage devices.

## Introduction

Research on material development as energy storage device was actively pursued for possible demotion of energy crisis of populated world. In this aspect electrochemical super capacitors (ECs) had attracted much interest due to their high power density, long cycle life, and higher energy density than conventional capacitors.[1-3] Particularly, nano crystalline metal oxides having pseudo capacitance, offer significant contribution to this technology due to capacitor like behaviour in electrochemical condition.[4-6] The modification of such specified properties of these materials will be fascinated by controlling the size, shape and phase selectivity. Tuning the shape of nano particles can remarkably change the activity and selectivity through the variations in surface atomic configurations and hence greatly effect on the morphology-dependent properties. Among all, ion oxides were chosen as electrode materials due to environment sustainability and cost effectiveness.[7,8] The high surface area and electrical conductivity of different phases of iron oxides enable it to make significant contribution as high capacitance in electrical double layer capacitors. Surface area of these materials can be enhanced either through size control or through self-assembling of nano building blocks. Generally these hierarchical structures were developed either by using self-assembled organic template media[8,9] or by utilizing the unique properties of organic solvents which influence the nucleation and growth of nanostructures[9-12] and the anisotropic properties of crystal nucleation and growth.[13] The main disadvantage of proposed various approaches were: difficulties in removal of organic contaminants along with generation of toxin. Therefore, challenges are still remain for simplified synthetic processes. Again

nanoparticles along with core/shell structure provide new properties based on the characteristics of each individual layer in a synergistic fashion. Since different form of iron oxides are formed either by olation-oxolation, dissolution-reprecipitation and dehydration mechanism[14] and also they have adsorptive properties, it was feasible to arrest growth of one phase being core and development of another phase in situ as shell by shielding the surface of primary phase with ligation or adsorption.

In this work, we develop a facile and greener method i.e. by using low cost, low toxic chemicals to fabricate novel flower like core shell iron oxide nano structures consisting of core shell through controlling the amount of solvents by a semi aqueous low temperature process where solvent act as both ligand and precipitating agent. The precipitation reactions were controlled by complexation process to get dispersed hierarchical structured materials in nano range. The different form of iron oxides such as ferrihydrite, goethite and hematite had been produced. Their electrochemical capacitance behaviour had been evaluated by using glassy carbon electrode and nafion (as one of the binder for the same). Up to now, the possibility of electrode fabricated from iron oxide powder on glassy carbon electrode with nafion as a binder as electrochemical capacitors has never been explored.

## Experimental

The chemicals used in the synthesis were analar grade; Fe $(NO_3)_3.9H_2O$ (Merck), Ethylene Glycol Mano Methyl Ether $(CH_3O.CH_2.CH_2.OH)$(Merck grade). The flowery shaped nano iron oxide precursors were prepared using a simple ligand mediation precipitation approach. In a typical procedure, required amount of ferric solution (0.1M) was taken in a three necked flask attached with condenser and pH meter, stirred for 15 min. Stock solution of EGME (ethylene glycol mono methyl ether) (0.2M) was added to the above solution with continuous stirring to form a homogeneous solution for another 10 min. After that the solution was heated to desired temperature for a fixed period, the flask was cooled down naturally to room temperature. The obtained precipitate was separated by centrifuge and rinsed several times using distilled water. Finally the product was dried at room temperature. Calcination was conducted in an electrical furnace in air at 400 °C for 4 h. Iron was analysed by volumetric method using BDAS indicator. To identify the crystal structures of the synthesized materials, XRD patterns were recorded with an automated Siemens D-5000 Diffractometer using Mo Kα (λ = 1.79 Å) radiation. The particle sizes of the prepared samples were studied by particle size analyser by Microtrac, Zetatrac. The IR spectra were taken using NICOLET-6700 Spectrometer. The morphology of the as-prepared samples was investigated by (TEM) (FEI, TECNAI $G^2$ 20, TWIN) operating at 200 kV, equipped with a GATAN CCD camera. The BET surface area was measured by an Autosorb-iQ and ASiQ-WiN device from Quanta chrome. The chemical states of the samples were analyzed by XPS, using a Thermo-VG Scientific ESCA Lab 250 microprobe with a monochromatic Al Kα X-ray source (1486.6 eV) and a typical energy resolution of 0.4-0.5 eV at full width at half maximum (FWHM). Collected XPS spectra were analysed using Casa-XPS software. All spectra were calibrated using the adventitious $C_{1s}$ peak with a fixed value of 284.8 eV. Cyclic-voltammograms were recorded using a computer controlled CHI660C electrochemical analyzer (CHI, USA). Electrochemical analyses were performed using two compartment three-electrode cell with a glassy carbon working electrode (area 0.07 $cm^2$), a calomel auxiliary electrode and Ag/AgCl (0.1M $Na_2SO_4$) as reference electrode in the potential range of 0 V to 0.8 V under a sweep rate of 5-100 mV/s. All the electrochemical experiments were carried out in an argon atmosphere. The as-synthesized materials were dispersed over glassy carbon electrode with 0.1ml of 2% Nafion and dried prior to electrochemical experiments. Cyclic voltammetries (CVs) were performed. Charge-discharge tests were performed by the same voltage range through chrono-potentiometric method. The electrochemical impedance spectroscopy (EIS) were recorded by applying a sine wave with amplitude of 10.0 mV over the frequency range from 1 MHz to 0.001 Hz.

## Result and Discussions

### Characteristics of as synthesised iron oxide

The two samples namely $Fe_1$ and $Fe_2$ were synthesized with solute to solvent ratio (Fe (III): EGME = 1:1 and 1:6 respectively) at $100^0$C and 5 hr of reaction time. The sample $Fe_2$ was heated at $400^0$C for 4hr for phase conversion named as $Fe_3$. As illustrated in Fig.1 (a), the crystalline peaks are identified as 2 line ferrihydrite ($Fe_1$), goethite ($Fe_2$), and hematite ($Fe_3$). The characteristic broad reflections of the 2LFh (2-Line ferrihydrite) phase at d-values of 2.58Å (110) and 1.54 Å (300) were matched with earlier reports.[14,15] When the solute to solvent ratio increased to 1:6, the XRD pattern of as prepared sample had shown peaks correspond to the planes at (110), (130),(101), (121), (131), (221), (151), (320) and (410) of goethite phase(JCPDS file: 00-029- 713). The low intensity with wide peaks for the α-FeOOH nanostructure might be attributed to low- crystallinity. The XRD of heated sample $Fe_3$ showed peaks at (012), (104), (110), (006), (113), (116), (018) and (208) planes for hematite phases (ICDD: 00-024-0072). The crystallite size was calculated using the Debye–Scherer formula. $D = 0{\cdot}9\lambda/\beta \cos\theta$, where D is the particle size, λ the wavelength of the X-ray used, β, θ are the half-width of X-ray diffraction lines and half diffraction angle of 2θ. The crystallite size was found to be 7.8 nm, 10.8 nm and 34.5 nm for $Fe_1$, $Fe_2$ and $Fe_3$ respectively. When the sample is heated the size of the particles increased. The lattice parameters of $Fe_1$, $Fe_2$, & $Fe_3$ were calculated as (a=4.75, b=9.994, c=3.16Å), (a=3.27, b=9.79, c=4.3Å) and (a=b=4.56, c=12.78Å) respectively. The sizes of the samples obtained from the particle size analyser were shown in Fig.1b were almost matching with XRD crystalline diameter confirming the size of the synthesized particle are in the nano range. The $Fe_1$ sample shows the particle size ranges from 10-50 nm while the $Fe_2$ shows 4-20 nm and the $Fe_3$ sample of particle size 20-50 nm. Faster agglomeration of ferrihydrite particle causes bigger size as compared to the goethite phase. Again the later phase was obtained at high ratio of solute to solvent was of lower particle size due to slow kinetics of precipitation.



 

Fig.1c showed the Mössbauer spectra of the iron oxides samples under study. The Mössbauer parameters of samples were given in Table 1. Spectrum of $Fe_1$ and $Fe_2$ showed a doublet and a combination of a singlet and a doublet respectively. The Mössbauer parameters of the singlet correspond to goethite (α-FeOOH) and that of doublet correspond to ferrihydrite. From the relative area of the two components we found that the major part of sample (about 70%) was goethite while rest was ferrihydrite. Heating the $Fe_2$ sample at 400°C favoured the formation of hematite. The Mössbauer spectrum of sample was showing almost 100% of the hematite phase. These results confirmed the observations from XRD results.

**Table 1** Mössbauer parameters of as synthesized iron oxide samples showing the sample $Fe_2$ had both goethite and hematite phases whereas sample $Fe_1$ and $Fe_3$ are monophasic iron oxide

| Sample | IS (mm/s) | QS (mm/s) | LW (mm/s) | HMF (T) | Area (%) | Phase |
|---|---|---|---|---|---|---|
| $Fe_1$ | 0.344 | 0.580 | 0.404 | | 100.0 | Ferrihydrite |
| $Fe_2$ | -0.004 | | 0.280 | | 80.5 | Goethite |
| | 0.352 | 0.523 | 0.461 | | 19.5 | Ferrihydrite |
| $Fe_3$ | 0.353 | -0.215 | 0.261 | 51.5 | 100.0 | Hematite |

The IR spectra were used to investigate any contamination by foreign materials, such as organic materials. For $Fe_1$ sample, the band shown in Fig.1d at 1654 $cm^{-1}$ was assigned to the O-H bending mode of water[16]. Cornell and Schwertmann[17] attributed band at 650 $cm^{-1}$ due to bulk OH deformations respectively. The weak peaks at 786 and 867 $cm^{-1}$ were attributed to the characteristic vibrations in the FeO–(OH) product.[18] The sharp spike at 1385 $cm^{-1}$ observed for the 2LFh sample can be attributed to $NO_3^-$ which was due to the ferric nitrate reagent used during synthesis.[17] In sample $Fe_2$, peaks for FeO–(OH) were very sharp and distinguished because of precipitation of goethite phase. The absorption bands at 551 and 474 $cm^{-1}$ in $Fe_3$ sample were assigned to Fe-O stretching and bending vibration mode of α-$Fe_2O_3$ respectively. There was no evidence that as synthesized particles were contaminated by foreign materials in the system, which was consistent with the XRD analysis results.

The XPS results provided information on surface and on bulk properties of iron oxide nano particles, as well as of aggregates. The $Fe_{2p}$ and $O_{1s}$ spectra were measured in the ranges between 705−735eV and 525−535eV respectively. For $Fe_1$ sample, a band for Fe($2P_{3/2}$) occurred at 711.6eV, indicating trivalent Fe[19] (Fig.1e). For $O_{1s}$ (Fig.1f), two peaks, at 530.3 and 531.7eV were attributed to $O_{1s}$ bound in ferric oxides[19] and to $O_{1s}$ coordinated in hydroxyl groups associated with Fe.[20] The latter peak was more intensified because of coordinated water molecule in ferrihydrite samples. For $Fe_2$ sample, the observed binding energies were 711.2 and 724.8eV assigned to Fe $2P_{3/2}$ and Fe $2P_{1/2}$ respectively. The binding energy in this sample was less as compared to previous sample due to presence of goethite phase. Due to electrostatic interactions between the photo-ionized $Fe_{2p}$ core hole and unpaired $Fe_{3d}$ electrons, spin–orbit coupling and crystal field interactions broad peaks were found. Additional satellite peaks were observed due to charge transfer and/or to shake-up processes. For this sample $O_{1s}$, the intensity of the peak at 530eV was more intense as compared to earlier sample of the peak, whereas intensity of the peak at 531.6eV was drastically diminished due to FeOOH form and also the same peak undergoes a slight red shift due to formation of the Fe-O(-O) bonds.[21] During sample calcination in $Fe_3$, the OH component decreases (due to dehydration) and an oxygen species appears about 530.3eV. It was likely due to differential charge effects if one takes into account the sample homogeneity and the fact that the oxygen sample treatments (calcination and reoxidation) were more likely to produce such effects in a sample like α-$Fe_2O_3$.

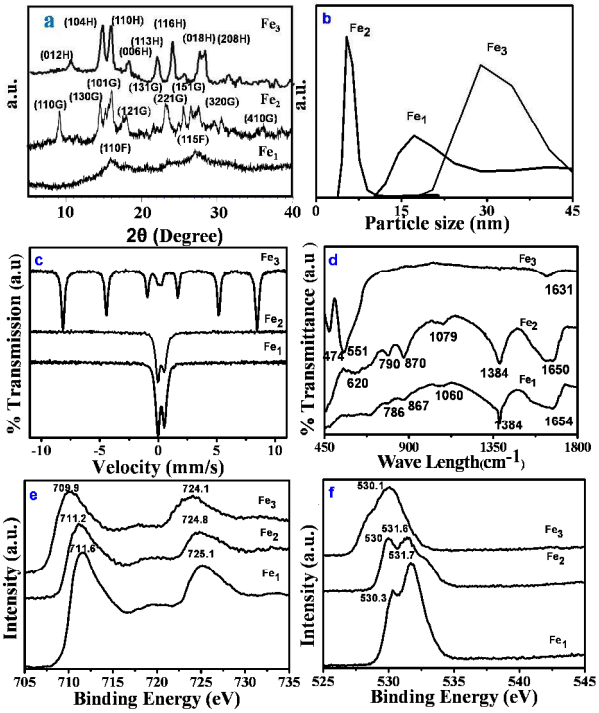


**Fig. 1** (a) XRD patterns, (b) Particle size distributions, (c) Mössbauer spectra, (d)IR spectra of iron oxide samples (e) XPS data for $Fe_{2p}$, and (f) XPS data for $O_{1s}$ of $Fe_1$, $Fe_2$ and $Fe_3$ iron oxide samples.

The aggregation of iron oxide nanoparticles into flowery structure was evidenced by the TEM analysis. The typical TEM images and lattice fringes/ selected area electron diffraction of the three different precursors $Fe_1$, $Fe_2$, & $Fe_3$ were shown in Fig.2. $Fe_1$ sample showed that small spherical nano particles were assembled and form a flower like structures and from the core, self-assembled spindle nano needles were growing. Misalignment of the needles on spherically structured arise may be due to the presence of crystalline defaults at

the grain interfaces, which could explain the small crystalline diameter obtained by XRD. The structure of the flowers also present filling defect holes possibly containing traces of solvents used for the synthesis. From the TEM picture, the presences of pores were also felt. This phenomenon could help in understanding the tiny misalignments in the flower crystalline structure. The role of the solvents in the formation of the complex flower-shaped structure seems decisive. SAED pattern of the $Fe_1$ displayed two bright rings at d value of 2.56 and 1.51 Å with shoulders on each side, identical to the 2-line ferrihydrite.[22] However, the TEM pictures obtained for $Fe_2$ sample showed complete flower-like morphologies. Most of the flowers showed an inner contrast variation, suggesting the existence of a core/shell structure, consistent with one form of iron oxide in core coated with other form of iron oxide. SAED patterns near centre and edge of the petals showed the planes

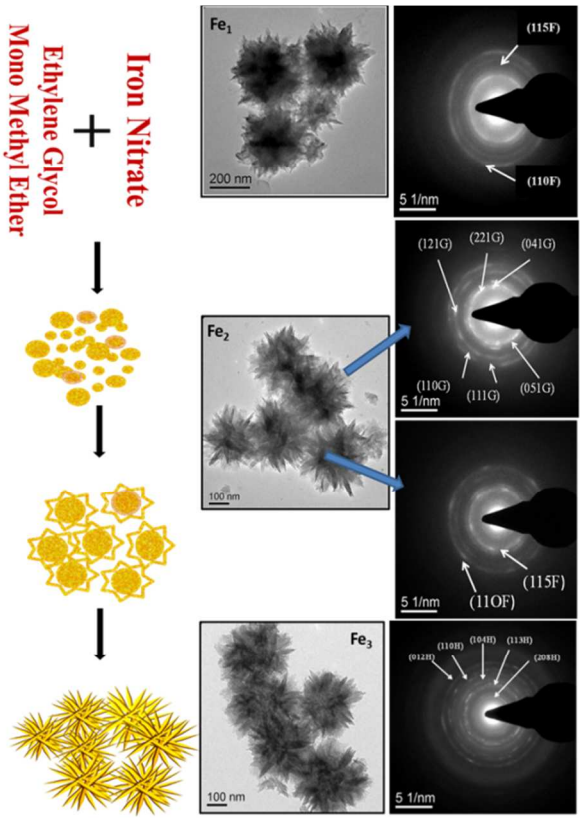


**Fig. 2** Growth models of as synthesised iron oxide flowers, shown in the left. The middle TEM image for $Fe_2$ shows EDAX images are different in core and boundary of the flowers confirming core-shell structure.

were different, the central part match to ferrihydrite phase whereas edge part match with goethite phase, which showed concentration of the reactant has a great impact both on the morphology as well as the phase purity of the nano particles. The synthesized nano goethite particles were changed to hematite phase after calcination at $400^0$C with retaining the sharper flowery shape with sharper needle like petals as shown in Fig.2c ($Fe_3$-sample). SAED pattern of $Fe_3$ samples shows all the diffraction patterns matched to hematite phase confirming complete conversation of goethite phase to hematite phase. A Schematic diagram for growth of nano flowers was included in the same figure.

Fig.3 showed the $N_2$ adsorption – desorption isotherms and the corresponding Barrett-Joyner-Halenda (BJH) pore size distribution curves. The Surface area of $Fe_1$, $Fe_2$, $Fe_3$ were 110.75 ($m^2$/g), 185 ($m^2$/g) and 58.72($m^2$/g) respectively. Surface area of goethite phase was more as compared to ferrihydrite phase may be due to delayed nucleation process which arised for strong complexation of solvent with iron ion. The sorption isotherms, in general, showed typical type IV isotherms according to the IUPAC classification. In $Fe_1$ and $Fe_2$ samples isotherm, multiple distinct capillary condensation steps can be seen from the inset of Fig. 3, which was typical characteristic of mesoporous material. The pore size distribution showed that the sample we obtained had a very narrow pore size distribution with an average pore diameter at about 3.8 nm. We think they were inter-particle pores. The formation of this mesoporous could be attributed to the generation of gaseous molecule during hydrolysis of iron complexes. The surface area of our obtained 2-lines ferrihydrite was very high. The amount adsorbed gradually increased at lower relative pressures and then increased sharply at higher relative pressures as shown in Fig. 3 for all the samples. This was in accordance with the characteristics of a type IV isotherm with a type H3 hysteresis loop associated with aggregates of plate like particles forming slit like pores. The observed hysteresis loop shifted to a higher relative pressure on approaching $P/P_0$= 1, suggesting the presence of mesoporous a low degree of aggregation, which was confirmed by TEM images (Fig. 2). The (BJH) calculation showed that the average pore radii were about 1.5-10 nm range for all the samples. From the above study all the samples showed a mesoporous distribution.[23-28]

**Formation mechanism**

Generally, the rate of nucleation and growth influenced the morphology of crystals. Here the development of flowery shape was a simplified self-assembling process, which could be understood as a result of a nucleation–oriented aggregation–recrystallization mechanism from primary nano crystals under solvated-complexation process. During synthesis condition precursor, $Fe(NO_3)_3{\cdot}9H_2O$ may react with 2-methoxyethanol to produce metal alkoxide, and the reaction can be expressed as follows :[29]

$$Fe(NO_3)_3 + 3CH_3OCH_2CH_2OH \rightarrow$$

$$Fe(OCH_2CH_2OCH_3)_3 + 3HNO_3 \quad (1)$$

Due to presence of water of crystallization in $Fe(NO_3)_3{\cdot}9H_2O$ and strong electro negativity of alkoxy, $Fe(OCH_2CH_2OCH_3)_3$ undergo hydrolysis and polymerisation to form gel, although water were mixed with 2-methoxyethanol. The alkoxide precursors then hydrolysed by following reactions:

$$Fe^{3+} + 3H_2O \rightarrow Fe(OH)_3 + 3H^+ \quad (2)$$

$$Fe(OH)_3 \rightarrow FeOOH + H_2O \quad (3)$$

$$2\ Fe(OH)_3 \rightarrow Fe_2O_3 + 3\ H_2O \quad (4)$$

Initially the spherically ferrihydrite nano particles were formed during nucleation process and then the solvated solution were tend to diffuse to the outer surface of ferrihydrite nano particle preventing their aggregation and acting themselves as the precursor for the

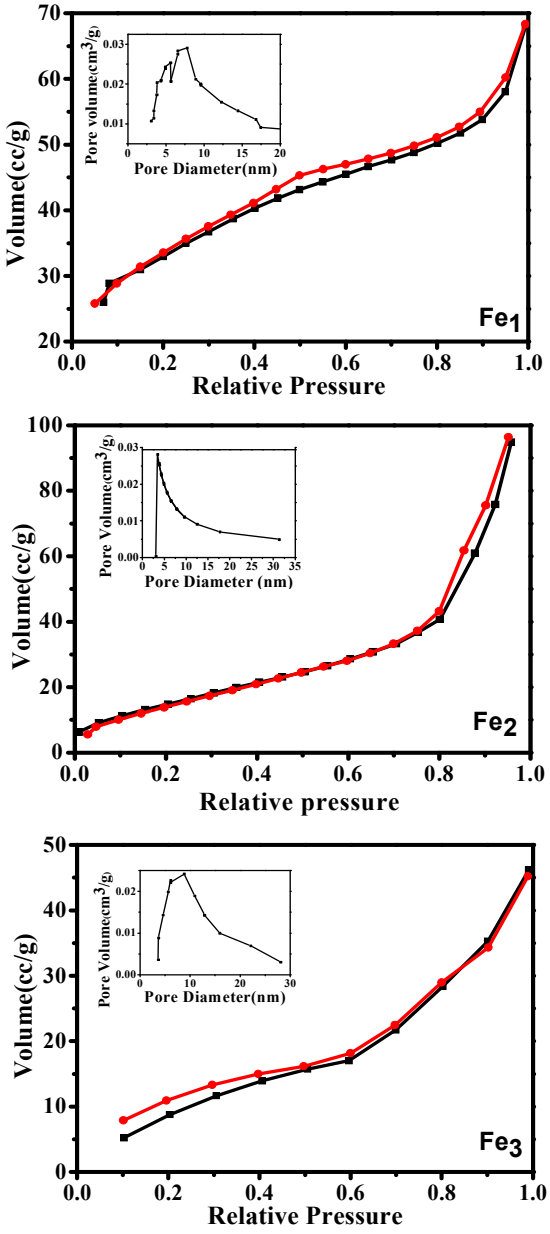


**Fig.3.** Surface areas and pore size distribution (inset Figs.) graphs of as synthesized iron oxides.

formation of petal like growth; several petals start to form from the same base (growth model shown in Fig. 2), which provides a site for the further growth of petals in the flower-shaped nanostructures by a self-catalytic process. The morphology of the deposited structures was more defined as the solvent concentration increases due to increase of complex solution and their surface diffusion in early formed ferrihydrite nano particles. During the growth process the petals likes outgrowth serve as a shell possibly due to homogeneity concentration gradient around the newly born nano particles.

**Cyclic voltammetry study**

The performance of our synthesised iron oxide product as electrode materials in supercapacitor is evaluated by cyclic voltammetry (CV) in three and two electrode system. Electrochemical studies of iron oxide were reported in several electrolytes, such as $Na_2SO_3$, $Na_2SO_4$, KOH and NaOH and it was found that an aqueous solution of $Na_2SO_4$ was the most suitable in the view of the maximum specific capacitance measured.[30-31] Accordingly, 0.1M $Na_2SO_4$ solution was used for electrochemical characterization in the present studies also. Here in we fabricated the electrode in a simplified process using nafion as binder. CV measurements were conducted to test the supercapacitor performances of flowery shaped 2LFh, core-shell α-FeOOH and hematite nano particles. CV curves of pristine nafion electrode and all synthesized iron oxides electrodes were obtained at 0.1M $Na_2SO_4$ solution between 0 to 0.8 V at a scan rate of 5mV/s Ag/AgCl). The CV curves for iron oxides/ nafion nano films and pristine nafion film vary greatly as shown in Fig.4a. The CV curve of nafion electrode did not show any rectangular curve. The electrode made up of with α-FeOOH predominantly showed rectangular shaped CV curve, strongly resembling the characteristics of an electrochemical double-layer, mostly observed for carbon based materials but also for faradaic pseudo-capacitance materials. It was notable that the CV curves retained their configurations with the increase of sweep rate (Figs.4b-4d), except that a positive shift of oxidation peaks and a negative shift of reduction peaks are observed, which was mainly due to the resistance of the electrodes. From all the CVs, a much larger integrated area of goethite core –shell phase film was observed. This pseudo-capacitance change may be due to adsorption of electrolyte cations ($Na^+$) on the electrode surface from electrolyte. Being amphoteric in nature of the iron oxide surface, $Na^+$ provides additional charge storage capacity. The capacitive current of iron oxides originates from the surface reaction of sulfate,

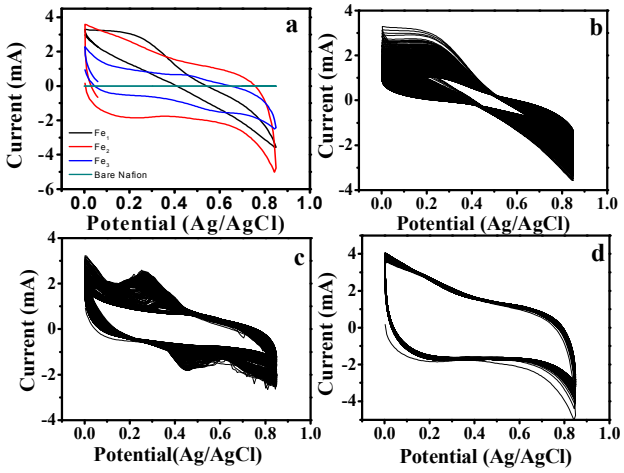


**Fig.4** Cyclic voltammetry curves for the iron oxide electrodes using 0.1 M $Na_2SO_4$ as electrolyte.(a) comparative CV of four electrodes at scan rate of 5 mV/s, (b) CV of sample $Fe_1$ for 200 cycle, (c) CV of sample $Fe_2$ for 200 cycle (d) CV of sample $Fe_3$ for 200 cycle.

as well as the charge compensation accompanied by intercalation of sulfate ions to balance the extra charge with the iron oxide layers. The nucleation centre for easy access of $SO_4^{2-}$ by the flowery iron oxide nano core can be guaranteed by the porous nature and thin thickness of the α-FeOOH shell. Therefore, both $Na^+$ and $SO_4^{2-}$ from the electrolyte were fully utilized in ferrihydrite α- FeOOH nano flower film. The decrease in specific capacitance was attributed to diffusion limits of electrolyte ions.[32-36] The results demonstrated the excellent reversibility and ideal pseudo-capacitive behaviour of the three electrodes. Despite that the curve shapes were similar, Fe addition within the oxides seemed to affect the enclosed area of the CV curves. The larger enclosed area implied that the higher energy density of the oxide could be achieved.[37] The specific capacitance of the supercapacitor can be determined from the charge/discharge test, using with the following equation:

$$Cs = I\,\Delta t / m\Delta V \qquad (5)$$

Where I is the discharge current, Δt is the discharging time period in seconds, m is the active mass and Δv is the potential difference.[38] The specific capacitance value for goethite core-shell nano flower was calculated to be 160 F/g. The capacitance of calcined $Fe_3$ hematite nano flower was calculated to be 200F/g. The specific capacitance for $Fe_1$ sample was not showing good behaviour as compared to other samples. Researchers have studied the specific capacitance of α-$Fe_2O_3$ with different electrolyte but with 0.1M $Na_2SO_4$ showed a good capacity at a scan rate of 5mV/s.[39] Specific capacitance of hematite at the same scan rate were reported; 116 F/g, 138 F/g, and 62 F/g were reported. [30,37,41]. In our study the specific capacitance was reasonably high in comparison with the values reported in the literature as shown in Table $S_1$. All the electrochemical capacitance value shown in the same table are obtained using three electrode systems. However, depending on the scan rate, the electrolytic system used in aqueous solutions and iron oxide composites with active material like graphene, activated carbon also affected the pseudo capacitance value. The cyclic performance of electrode was also investigated by CV. Charge–discharge up to 200 cycles for $Fe_1$, $Fe_2$ and $Fe_3$ iron oxide electrodes at the current density 5 mA/g were shown in Fig.4b, c and d respectively. It could be seen that the CV could maintain a good symmetry. This indicates that the electrode had regular capacitive behaviour and good cycling stability.[40] Charge–discharge up to 10 cycles for all the iron oxide electrodes at the current density 5 mA/g were shown in Fig.5. The potential–time relationships on charge–discharge profiles were all approximately linear. This indicates that the electrode had regular capacitive behaviour and good cycling stability. The discharging capacity slightly increased with number of cycle for core shell goethite and hematite particle whereas for 2L Ferrihydrite the same remain constant for 10 cycle of study. Cycling stability of $Fe_2$ and $Fe_3$ electrodes were examined for 500 cycles at a specific current density of (Fig.5d) 5 mA/g. The specific capacitance slightly decreased for $Fe_2$ sample where for $Fe_3$ sample the value remain almost constant. For practical view point we had tested the sample $Fe_3$ in two electrode system at different scan rates. Specific capacitance of 82.6 F/g was calculated at a scan rate of 200 mV/s in two electrode system at as shown in Fig. 6a. Charge–discharge up to 3 cycles in two electrode system at a scan rate of 200 mV/s was shown in Fig.6b. To further understand the electrochemical performance characteristics, we reported the electrochemical impedance spectroscopy (EIS) carried out at open circuit potential with an ac perturbation of 10 mV in the frequency range of 1 MHz to

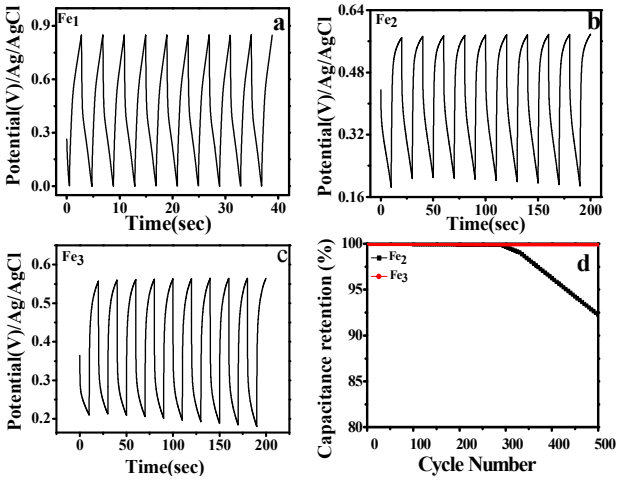


**Fig.5** Typical charge-discharge plots for (a) $Fe_1$, (b) $Fe_2$, and (c) $Fe_3$ samples at current density 5mA/g. The iron oxide supercapacitor exhibits good electrochemical capacitance performance, demonstrated by a linear variation of the voltage during the charging-discharging process. (d) % retention of specific capacitance as a function of cyclic number.

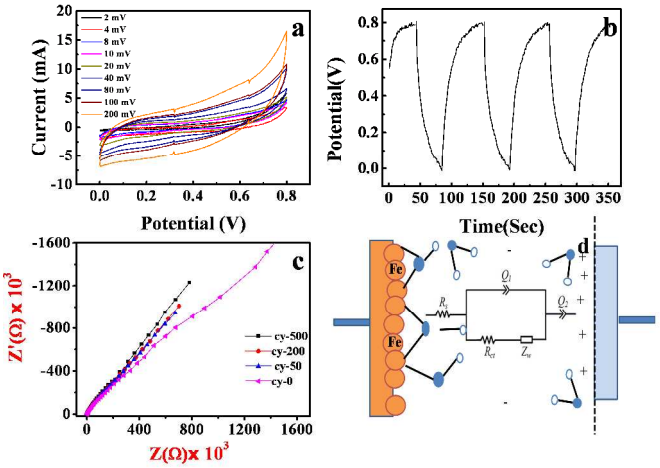


**Fig. 6** (a) Cyclic voltammograms of sample $Fe_3$ electrode in two electrode system. Data was collected under a Ar(g) atmosphere, (b)Charge-discharge curves measured at 200 mV/s, (c) Nyquist plot of electrode made from sample $Fe_3$. And (d) Schematic view of the iron oxide/electrolyte interface in the electrode setup and the equivalent circuit model used for EIS modelling. The equivalent circuit model consists of the solid phase and the aqueous phase. The following circuit components: solution resistance ($R_s$), a double layer capacitance (Cdl), and a CPE as well as a resistance ($R_{film}$) for charge-carrier transfer from the diffuse to the compact layer is considered.

0.001 Hz. Figs. 6c and d showed the Nyquist plots thus obtained. The EIS data were fitted (EIS original data for cycle-200 and its fitted data were shown in supporting Fig. $S_1$) based on an equivalent circuit model consisting of bulk solution resistance Rs, charge-transfer resistance $R_{film}$, and double-layer capacitance Cdl. EIS data revealed that the hematite flowery sample electrodes showed that increasing cycles had more effect on lowering impedance with much smaller $R_{film}$. The parameters of EIS was shown in Table $S_2$. It was observed that the resistance of the electrode was greatly decreased after cycling, indicating a better conductivity and fast ionic charge/discharge process between the electrode and electrolyte. The slope of the low frequency part of the EIS curve after cycling was increased slightly as the number of cycles increased, which revealed a better ability of energy storage. The Cdl increased after cycling, indicating a much better performance.

## Conclusion

We have reported a facile in-situ synthetic approach towards the development of iron oxide flowery shaped self-assembled nano particle. The above study was quite helpful for developing different phases of flowery shape iron oxides along with core shell flowery structure by controlling only the solute to solvent ratio which in turn controls both hydrolysis and selective phase precipitation. The particle sizes were uniform varies between 10-100nm with meso-porous structure. The samples were further explored for the electrochemical behaviour which confirmed that the iron oxide synthesized under optimum conditions also had a good rate capability. It exhibited high specific capacitance (200 F/g at current density of 5 mA/g), and long-term cycling stability (99.9% at 5 mA/g after 500 cycles), The pure iron oxide nano materials having good capacitance along with charge –discharge behaviour without further hybridisation or addition of dopant in nano structured material. The simple synthetic one step approach and the novel fabrication of electrode without other active material may offer promising approach for practical applications including Li-ion batteries, electro catalysis, and heterogeneous catalysis.

## Acknowledgement

The authors were very much tankful to Prof. B.K. Mishra, Director, IMMT, Bhubaneswar for his kind permission and encouragement for doing this study. First author was very much obliged to DST-India (Inspire Division) for their support and encouragement as funding agency for doing research work**.**

## Notes and references

[a] Institute of Minerals and Materials Technology

Electronic Supplementary Information (ESI) available: [details of any supplementary information available should be included here]. See DOI: 10.1039/b000000x/

## References

1 W. Zhou, X. Cao, Z. Zeng, W. Shi, Y. Zhu, Q. Yan, H. Liu, J. Wang and H. Zhang, *Energy Environ. Sci*., 2013, **6**, 2216.

2 S. L. Kuo, N. L. Wu, *J. Power Sources*, 2006, **162**, 1437.

3 W. Wei, X. Huang, Y. Tao, K. Chen and X. Tang, *Phys. Chem. Chem. Phys.*, 2012, **14**, 5966.

4 R. L. Doyle and M. E. G. Lyons, *Phys. Chem. Chem. Phys*., 2013, **15**, 5224.

5 M. B. Sassin, A. N. Mansour, K. A. Pettigrew, D. R. Rolison and J. W. Long, *ACS Nano,* 2010, **4**, 4505.

6 C. M. Ban, Z. C. Wu, D. T. Gillaspie, L. Chen, Y. F. Yan, J. L. Blackburn and A.C. Dillon, *Adv. Mater*., 2010, **22**, 145.

7 Z. Yu, F. Gao, J. Wang, H. Pang and Q. Lu, *Angew. Chem*., 2010, **122**, 6472.

8 J. S. Chen, T. Zhu, X. H. Yang, H.G. Yang and X.W. Lou, *J. Am. Chem. Soc*., 2010, **20**, 13162.

9 L. J. Liu, J. G. Guan, W. D. Shi, Z. G. Sun and J. S. Zhao, J. Phys. Chem. C, 2010, **114**, 13565.

10 X. Huang, J. Guan, Z. Xiao, G. Tong, F. Moua and X. Fan, *J. Colloid and Interface Science*, 2011, **357**, 36.

11 F. Z. Mou, J. G. Guan, Z. G. Sun, .A. Fan and G.X. Tong, *J. Solid State Chem*. 2010, **183,** 736.

12 L. Y. Chen, Z. D. Zhang and W. Z. Wang, *J. Phys. Chem. C*, 2008, **112**, 4117.

13 Z. Wang, H.S. Gu, Y.M. Hu, K. Yang, M.Z. Hu, D. Zhou, and J.G. Guan *Cryst Eng Comm.,* 2010, **12,** 3157.

14 K. Rout, M. Mohapatra, S. Anand, *Dalton Trans.*, 2012, **41**, 3302.

15 T. Mathew, K. Suzuki, Y. Nagai, T. Nonaka,Y. Ikuta, N. Takahashi, N. Suzuki and H. Shinjoh, *Chem. Eur. J* , 2011, **17** 1092.

16 H. Zhang, M. Bayne, S. Fernando, B. Legg, M. Zhu, R. L. Penn and J. F. Banfield, *J. Phys. Chem. C*, 2011, **115**, 17704.

17 R. M. Cornell and U. Schwertmann, The Iron Oxides: Structure, Properties, Reactions. Wiley VCH, 2003.

18 G. E. J. Poinern, D. Parsonage, T. B. Issa, M.K. Ghosh, E. Paling and P. Singh, *International J. Engineering*, 2010, **2,** 13.

19 E. McCaffertyand, J. P. Wightman, *Surf Interface Anal*, 1998, **26**, 549.

20 R. K. Vempati, R. H. Loeppert, D. C. Duffner and D. L. Cocke, *Soil Sci. Soc. of America Journal,* 1990, **54,** 695.

21 G. Kataby, A. Ulman, R. Prozorov and A. Gedanken, *Langmuir*, 1998, **14**, 1512.

22 D. E. Janney, J. M. Cowley and P. R. C. Buseck, *Clay Minerals*, 2000, **48**, 111.

23 H. Liu, J. Xie and K. Wang, *J. Alloy Compd.*, 2008, **459**, 521-525.

24 J. K. Shon, S. S. Kong, S. S. Kim, M.S. Kang, J. Man, *Functional Materials Letters,* 2008, **1,** 151.

25 S. Yang, Y. Sun, L. Chen, L. Hernandez, X. Feng, K. Mullen, *Scientific reports,* 2012, **2,** 427.

26 G. Zhou, D. W. Wang, X. Li, L. Zhang, N. Li, Z. S. Wu, L. S. Wen, G. Qing, M. Lu, H. M. Cheng, *Chem. Mater*, 2010, **22** 5306.

27 Y. Zhang, H. Feng, X. B. Wu, L. Z. Wang, A. Q. Zhang and T. C. Xia, Int. J. Hydrogen Energy, 2009, **34**, 4889.

28 Y. S. Li, J. S. Church and A. L. Woodhead, *J. Magnetism and Magnetic Materials,* 2012, **324**, 1543.

29 L. Legrand, G. Sagon, S. Lecomte, A. Chausse and R.A. Messina, *Corros. Sci*., 2001, **43**, 1739.

30 S. Shivakumara, T. R. Penki and N. Munichandraiah, *ECS Electrochemistry Letters,* 2013, **2**, 60.

31 J. Chen, K. Huang and S. Liu, *Electrochimcal Acta*, 2009, **55**, 1.

32 G. Tong, J. Guan and Q. Zhang, *Materials Chemistry and Physics*, 2011, **127**, 371.

33 Z. C. Li, M. Y. Guan, Z. S. Lou and T. M. Shang, *Micro & Nano Letters,* 2012, **7,** 33.

34 Q. Shou, J. Cheng, L. Zhang, B.J. Nelson and X. Zhang, *J. Solid State Chemistry,* 2012, **185**, 191.

35 L. Dghoughi, B. Elidrissi, C. Bernede, M. Addou, M. A. Lamrani and M. R. H. Erguig *Applied Surface Science*, 2006, **253,** 1823,.

36 N. L. Wu, S. Y. Wang, C. Y. Han, D. S. Wu, L. R. Shiue, *J. Power Sources*, 2003, **113**, 173.

37 D. Wang, Q. Wang and T. Wang, *Nanotechnology,* 2011, **22,** 135604.

38 Y. Zhang, H. Feng, X. B. Wu, L. Z. Wang, A. Q. Zhang and T. C. Xia, *Int. J. Hydrogen Energy,* 2009, **34**, 4889.

39 D. Liu, X. Wang, X. Wang, W. Tian, J. Liu, C. Zhi, D. He and Y. B. D. Golberg, *J. Mater. Chem.*, 2013, **1**, 1952.

40 H. Zhang, Y. Wang, C. Liu and H. Jiang, *J. Alloys and Compounds*, 2012, **517**, 1.

41 K. Xie, J. Li, Y. Lai, et al., *Electrochem. Commun*., 2011, **13**, 657.



 